Received February 15, 2021, accepted February 25, 2021, date of publication March 1, 2021, date of current version March 26, 2021.

Digital Object Identifier 10.1109/ACCESS.2021.3062942

Complex Envelope Approximate Crank-Nicolson Method and Its Open Boundary Implementation for Bandpass Problem

SHIHONG WU[1], YUNYUN DONG[1], FENG SU[1], LINING LIU[1], AND XIANGGUANG CHEN[1,2]

[1]Department of Electrical and Electronic Engineering, College of Engineering, Yantai Nanshan University, Longkou 265713, China
[2]School of Chemistry and Chemical Engineering, Beijing Institute of Technology, Beijing 100081, China

Corresponding author: Shihong Wu (shihongwu@hotmail.co.jp)

This work was supported in part by the National Natural Science Foundation of Shandong under Grant ZR2016FM28, and in part by the Double Hundred Plan Talent Project of Yantai.

ABSTRACT To efficiently simulate the bandpass electromagnetic problems by employing the finite-difference time-domain (FDTD) algorithm, unconditionally stable implementation is proposed based upon the complex envelope method and the Crank-Nicolson Direct-Splitting (CNDS) algorithm. To further absorb outgoing waves and reduce wave reflections in open region problems, absorbing boundary condition with improved absorption is proposed by incorporating the proposed scheme with the higher order perfectly matched layer (PML) formulation. The proposed scheme takes advantage of the complex envelope method, the CNDS algorithm and the higher order PML formulation in terms of simulating bandpass signals and enhancing absorption and improving computational efficiency. Numerical examples are carried out to further demonstrate the effectiveness and efficiency. Through the resultants, it can be illustrated that the proposed scheme can not only obtain considerable accuracy, favorable absorbing performance, outstanding efficiency in the simulation of bandpass open region problems but also maintain the stability of the algorithm when the time step surpasses far beyond the Courant-Friedrich-Levy condition.

INDEX TERMS Complex envelope (CE), Crank-Nicolson direct-splitting, finite-difference time-domain (FDTD), perfectly matched layer (PML).

I. INTRODUCTION

With outstanding advantages in simulating electromagnetic problems, the finite-difference time-domain (FDTD) algorithm has gained considerable attention in past recent decades [1]–[4]. The time and spatial sampling of the conventional FDTD is based on the lowpass-limited sampling theorem which has been verified to be inefficient in bandpass simulation [5]. The reason is that the time step must be calculated according to the maximum frequency resulting in the degeneration of efficiency and accuracy when calculating bandpass signals [1], [6]. In order to alleviate such phenomenon and overcome such drawback, the complex envelope (CE) method is introduced into the implementation. Based on the bandpass-limited sampling theorem, the time step of CE-FDTD algorithm can be calculated according to the bandwidth rather than the maximum frequency [7], [8]. That means the time step of the CE-FDTD algorithm can be enlarged for several times compared with the conventional FDTD algorithms.

As a time explicit algorithm, the stability of the conventional FDTD algorithm is severely limited by the Courant-Friedrich-Levy (CFL) condition [9]. By employing the FDTD algorithm to the large amount of time step problems, the simulation duration will be unacceptable. Unconditionally stable algorithms are carried out to remove the CFL condition and improve the efficiency during the calculation. The Crank-Nicolson (CN) scheme which can obtain the solution of equations accurately has gained considerable attention [10]. The original CN scheme can merely solve the Maxwell's equations in one-dimensional problems [11]. In multi-dimensional problems, large sparse matrices will be formed resulting in the computation much more expensive [12]. Thus, a series of approximate CN algorithms are developed in two-dimensions, such as CN approximate-decoupling and CN Douglas-Gunn [13], [14]. It should be

The associate editor coordinating the review of this manuscript and approving it for publication was Chan Hwang See.

noticed that the approximate CN algorithms in 2-D cases cannot be expanded to 3-D cases directly [15]. Recently, CN cycle-sweep (CS), CN approximate-factorization-splitting (AFS) and CN direct-splitting (DS) schemes are introduced to three-dimensions [16], [17]. However, it has been proven that CNCS is a conditionally stable implementation [18], [19]. The CNAFS scheme is implemented by adding higher order disturbance terms at both sides of the equations. Thus, the resultants can be spitted by the AFS procedure into three sub-steps resulting in the forming of three tri-diagonal matrices of each components which can be efficiently solved by the Thomas decomposition [20], [21]. According to the CNDS scheme, the field matrices can be spitted by two sub-steps. By approximating the coupled equations, each field can be solved by two tri-diagonal matrices of each components. Furthermore, by introducing moderate auxiliary variables, the efficiency can be further improved [19]. Compared with CNDS and CNAFS schemes, it can be concluded that the CNDS scheme can obtain better computational efficiency, considerable accuracy and outstanding absorption during the simulation [19], [20].

To solve different kinds of open region problems, absorbing boundary condition must be introduced to terminate unbounded lattice. The perfectly matched layer (PML) is regarded as the most powerful ones [22]. As the Berenger's PML is implemented by split-field formulation, several auxiliary variables should be introduced resulting in the decrement of efficiency and absorbing performance. To not only overcome such problem but also improve the accuracy, the stretched coordinate PML (SC-PML) and complex-frequency-shifted (CFS) PML schemes are proposed [23], [24]. The SC-PML and CFS-PML have advantages of simplifying the implementation at the corners and edges of the PML regions, reducing late-time reflections and attenuating low-frequency evanescent waves, respectively [23], [25]. In order to further improve the calculation accuracy, the higher order FDTD is incorporated with PML formulation [26]. However, by employing them to low-frequency problems, it has been demonstrated that the absorbing performance becomes unacceptable. The reason is that the low-frequency propagation waves cannot be efficiently absorbed [27]. Thus, the higher order PML is carried out not only to alleviate such problem but also to further enhance the absorbing performance [28].

Until now, several published works which combine the approximate CN algorithms and higher order PML are mainly focus on the 2-D situations [29], [30]. Although CNAFS-PML and CNDS-PML schemes are proposed [19], [20], they are implemented by CFS-PML according to the lowpass-limited sampling theorem. Thus, they are inefficiency in low-frequency and bandpass problems.

Here, based upon the CE method, the higher order PML formulation and the CNDS algorithm, unconditionally stable higher order CNDS-PML is proposed for bandpass open region problems, denoted as CE-CNDS-HO-PML. Numerical examples are carried out in 3-D cases for the further demonstration.

II. FORMULATION

For simplifying the equations without losing the generality, E_x and H_z are chosen as examples for the demonstration of the formulation In the higher order PML regions, the source-free Maxwell's equations in the frequency domain can be written as

$$j\omega\varepsilon_0 E_x = S_y^{-1}\partial_y H_z - S_z^{-1}\partial_z H_y \tag{1}$$

$$-j\omega\mu_0 H_y = S_z^{-1}\partial_z E_x - S_x^{-1}\partial_x E_z \tag{2}$$

where S_η, $\eta = x, y, z$ is the higher order stretched coordinate variables with CFS factor which can be defined as

$$S_\eta = \left(\kappa_{\eta 1} + \frac{\sigma_{\eta 1}}{\alpha_{\eta 1} + j\omega\varepsilon_0}\right)\left(\kappa_{\eta 2} + \frac{\sigma_{\eta 2}}{\alpha_{\eta 2} + j\omega\varepsilon_0}\right) \tag{3}$$

where $\kappa_{\eta n}, n = 1, 2$ is selected as $\kappa_{\eta n} \geq 1$, $\sigma_{\eta n}$ and $\alpha_{\eta n}$ are positive real. By employing the partial fraction method, S_η^{-1} can be given as

$$S_\eta^{-1} = k_\eta \frac{j\omega + a_{\eta 1}}{j\omega + b_{\eta 1}} \frac{j\omega + a_{\eta 2}}{j\omega + b_{\eta 2}} \tag{4}$$

where $\kappa_\eta = 1/(\kappa_{\eta 1}\kappa_{\eta 2})$, $a_{\eta n} = \alpha_{\eta n}/\varepsilon_0$ and $b_{\eta n} = a_{\eta n} + a_{\eta n}/\kappa_{\eta n}$. By substituting (4) into (1) and (2), one obtains

$$j\omega\varepsilon_0 E_x = k_y \frac{j\omega + a_{y1}}{j\omega + b_{y1}} \frac{j\omega + a_{y2}}{j\omega + b_{y2}} \frac{\partial H_z}{\partial y} - k_z \frac{j\omega + a_{z1}}{j\omega + b_{z1}} \frac{j\omega + a_{z2}}{j\omega + b_{z2}} \frac{\partial H_y}{\partial z} \tag{5}$$

$$j\omega\mu_0 H_y = k_x \frac{j\omega + a_{x1}}{j\omega + b_{x1}} \frac{j\omega + a_{x2}}{j\omega + b_{x2}} \frac{\partial E_z}{\partial x} - k_z \frac{j\omega + a_{z1}}{j\omega + b_{z1}} \frac{j\omega + a_{z2}}{j\omega + b_{z2}} \frac{\partial E_x}{\partial z} \tag{6}$$

By introducing the auxiliary variables $F_{x\eta n}$ and $G_{y\eta n}$ into the equations (5) and (6), one obtains

$$j\omega\varepsilon_0 E_x = (j\omega + a_{y1}) F_{xy2} - (j\omega + a_{z1}) F_{xz2} \tag{7}$$

$$j\omega\mu_0 H_y = (j\omega + a_{x1}) G_{yx2} - (j\omega + a_{z1}) G_{yz2} \tag{8}$$

where the auxiliary variables $F_{x\eta n}$ and $G_{y\eta n}$ almost have the similar forms, $F_{x\eta n}$ are given as examples, written as

$$\begin{aligned} F_{x\eta 1} &= k_\eta \frac{1}{j\omega + b_{\eta 1}} \frac{\partial H_{\tilde{\eta}}}{\partial \eta} \Rightarrow j\omega F_{x\eta 1} + b_{\eta 1} F_{x\eta 1} \\ &= k_\eta \partial_\eta H_{\tilde{\eta}} \end{aligned} \tag{9}$$

$$\begin{aligned} F_{x\eta 2} &= \frac{j\omega + a_{\eta 2}}{j\omega + b_{\eta 2}} F_{x\eta 1} \Rightarrow j\omega F_{x\eta 2} + b_{\eta 2} F_{x\eta 2} \\ &= j\omega F_{x\eta 1} + a_{\eta 2} F_{x\eta 1} \end{aligned} \tag{10}$$

where $\tilde{\eta}$ is the complement of η, for example, when calculating E_x, $\eta = y$ while $\tilde{\eta} = z$. By substituting (9)-(10) to (7)-(8), one obtains

$$\begin{aligned} j\omega\varepsilon_0 E_x = {} & (a_{y2} - b_{y1}) F_{xy1} + (a_{y1} - b_{y2}) F_{xy2} + k_y \partial_y H_z \\ & - (a_{z2} - b_{z1}) F_{zx1} - (a_{z1} - b_{z2}) F_{zx2} - k_z \partial_z H_y \end{aligned} \tag{11}$$

$$j\omega\mu_0 H_y = (a_{x2} - b_{x1})\, G_{yx1} + (a_{x1} - b_{x2})\, G_{yx2} + k_x \partial_x E_z - (a_{z2} - b_{z1})\, F_{zx1} - (a_{z1} - b_{z2})\, F_{zx2} - k_z \partial_z H_y \tag{12}$$

By employing the CE method, bandpass signal can be expressed as the following expression as $\Phi = Re\left\{\hat{\Phi} e^{j\varpi t}\right\}$, where the operator $Re\{\cdot\}$ represents the real part of the equation, ϖ is the carrier frequency, Φ is the original field component and $\hat{\Phi}$ is the CE bandpass signal. By transforming (11-12) into the time domain according to the relationship $j\omega \leftrightarrow \partial/\partial t$, rewriting the resultants according to the CE method and rearranging the resultants, one obtains

$$\begin{aligned}\hat{E}_x^{n+1} &= c_1 \hat{E}_x^n + p_{1ey}\hat{F}_{xy1}^n + p_{2ey}\hat{F}_{xy2}^n \\ &\quad + p_{3ey}\delta_y\left(\hat{H}_z^{n+1} + \hat{H}_z^n\right) \\ &\quad - p_{1ez}\hat{F}_{xz1}^n - p_{2ez}\hat{F}_{xz2}^n - p_{3ez}\delta_z\left(\hat{H}_y^{n+1} + \hat{H}_y^n\right) \quad (13)\\ \hat{H}_y^{n+1} &= c_1 \hat{H}_y^n + p_{1hx}\hat{G}_{yx1}^n + p_{2hx}\hat{G}_{yx2}^n \\ &\quad + p_{3hx}\delta_x\left(\hat{E}_z^{n+1} + \hat{E}_z^n\right) \\ &\quad - p_{1hz}\hat{G}_{yz1}^n - p_{2hz}\hat{G}_{yz2}^n - p_{3hz}\delta_z\left(\hat{E}_x^{n+1} + \hat{E}_x^n\right) \quad (14)\end{aligned}$$

where $c_1 = (2 - j\varpi\Delta t)/(2 + j\varpi\Delta t)$, $c_2 = 1/(2 + j\varpi\Delta t)$, $p_{1e\eta} = 2c_2\Delta t\left(a_{\eta 2} - b_{\eta 1}\right)/\varepsilon_0$, $p_{2e\eta} = 2c_2\Delta t\left(a_{\eta 1} - b_{\eta 2}\right)/\varepsilon_0$, $p_{3e\eta} = 2c_2\Delta t k_\eta/\varepsilon_0$, $p_{1h\eta} = 2c_2\Delta t\left(a_{\eta 2} - b_{\eta 1}\right)/\mu_0$, $p_{2h\eta} = 2c_2\Delta t\left(a_{\eta 1} - b_{\eta 2}\right)/\mu_0$ and $p_{3h\eta} = 2c_2\Delta t k_\eta/\mu_0$. The operator δ_η is the first order finite-difference form by employing the CN scheme, for example,

$$\delta_y \hat{H}_z^n = \left(\hat{H}_z^n\Big|_{i+1/2,j+1/2,k} - \hat{H}_z^n\Big|_{i+1/2,j-1/2,k}\right)\Big/(2\Delta y) \tag{15}$$

The auxiliary variables can be given according to the CE method in the time domain as

$$\hat{F}_{x\eta 1}^{n+1} = p_{4\eta}\hat{F}_{x\eta 1}^n + p_{5\eta}\delta_\eta \hat{H}_{\tilde{\eta}} \tag{16}$$

$$(j\varpi + \partial_t)\,\hat{F}_{x\eta 2} + b_{\eta 2}\hat{F}_{x\eta 2} = (j\varpi + \partial_t)\,\hat{F}_{x\eta 1} + a_{\eta 2}\hat{F}_{x\eta 1} \tag{17}$$

where $p_{4\eta} = \left(2 - j\varpi\Delta t - b_{\eta 1}\Delta t\right)/\left(2 + j\varpi\Delta t + b_{\eta 1}\Delta t\right)$, $p_{5\eta} = 2\Delta t k_\eta/\left(2 + j\varpi\Delta t + b_{\eta 1}\Delta t\right)$, $p_{6\eta} = \left(2 - j\varpi\Delta t - b_{\eta 2}\Delta t\right)/\left(2 + j\varpi\Delta t + b_{\eta 2}\Delta t\right)$, $p_{7\eta} = \left(2 + j\varpi\Delta t + a_{\eta 2}\Delta t\right)/\left(2 + j\varpi\Delta t + b_{\eta 2}\Delta t\right)$ and $p_{8\eta} = \left(2 - j\varpi\Delta t - a_{\eta 2}\Delta t\right)/\left(2 + j\varpi\Delta t + b_{\eta 2}\Delta t\right)$. It can be observed that the coupled equations can be updated by employing (13)-(14) directly. By this means, large sparse matrices will form during each iteration steps resulting in the computation much more expensive which becomes unrealistic sometimes. Thus, the CNDS-FDTD algorithm is proposed to alleviate such phenomenon. Equations (13)-(14) can be given in the matrix form as

$$(I - D_1 - D_2)\,\hat{\Phi}^{n+1} = (I_1 + D_1 + D_2)\,\hat{\Phi}^n + \hat{A}^n \tag{18}$$

where I is the identity matrix, $I_1 = c_1 I$, $\hat{A}^n$ is the other terms at nth time step, $\hat{\Phi} = \left(\hat{E}_x, \hat{E}_y, \hat{E}_z, \hat{H}_x, \hat{H}_y, \hat{H}_z\right)^T$,

$$D_1 = \begin{bmatrix} 0 & 0 & 0 & 0 & -p_{3ez}\delta_z & 0 \\ 0 & 0 & 0 & 0 & 0 & -p_{3ex}\delta_x \\ 0 & 0 & 0 & -p_{3ey}\delta_y & 0 & 0 \\ 0 & 0 & -p_{3hy}\delta_y & 0 & 0 & 0 \\ -p_{3hz}\delta_z & 0 & 0 & 0 & 0 & 0 \\ 0 & -p_{3hx}\delta_x & 0 & 0 & 0 & 0 \end{bmatrix},$$

and $D_2 = \begin{bmatrix} 0 & 0 & 0 & 0 & 0 & p_{3ey}\delta_y \\ 0 & 0 & 0 & p_{3ez}\delta_z & 0 & 0 \\ 0 & 0 & 0 & 0 & p_{3ex}\delta_x & 0 \\ 0 & p_{3hz}\delta_z & 0 & 0 & 0 & 0 \\ 0 & 0 & p_{3hx}\delta_x & 0 & 0 & 0 \\ p_{3hy}\delta_y & 0 & 0 & 0 & 0 & 0 \end{bmatrix}$.

According to the CNDS procedure, the disturbances terms $\mathbf{D_1 D_2}\hat{\Phi}^{n+1}$ and $\mathbf{D_1 D_2}\hat{\Phi}^{\mathbf{n}}$ are added at both sides of the equations. The resultants can be given as

$$(\mathbf{I} - \mathbf{D_1})\,\hat{\Phi}^* = (\mathbf{I_1} + \mathbf{D_1} + 2\mathbf{D_2})\,\hat{\Phi}^{\mathbf{n}} + \hat{\mathbf{A}}^{\mathbf{n}} \tag{19}$$

$$(\mathbf{I} - \mathbf{D_2})\,\hat{\Phi}^{n+1} = \hat{\Phi}^* - \mathbf{D_2}\hat{\Phi}^{\mathbf{n}} \tag{20}$$

By expanding the equations for upation, one obtains

$$\begin{aligned}\hat{E}_x^* &= c_1\hat{E}_x^n - p_{3ez}\partial_z\left(\hat{H}_y^* + \hat{H}_y^n\right) + 2p_{3ey}\partial_y\hat{H}_z^n \\ &\quad + p_{1ey}\hat{F}_{xy1}^n + p_{2ey}\hat{F}_{xy2}^n - p_{1ez}\hat{F}_{xz1}^n - p_{2ez}\hat{F}_{xz2}^n \quad (21)\\ \hat{H}_y^* &= c_1\hat{H}_y^n - p_{3hz}\partial_z\left(\hat{E}_x^* + \hat{E}_x^n\right) + 2p_{3hx}\partial_x\hat{E}_z^n \\ &\quad + p_{1hx}\hat{G}_{yx1}^n + p_{2hx}\hat{G}_{yx2}^n - p_{1hz}\hat{G}_{yz1}^n - p_{2hz}\hat{G}_{yz2}^n \quad (22)\\ \hat{E}_x^{n+1} &= \hat{E}_x^* + p_{3ey}\partial_y\left(\hat{H}_z^{n+1} + \hat{H}_z^n\right) \quad (23)\\ \hat{H}_y^{n+1} &= \hat{H}_y^* + p_{3hx}\partial_x\left(\hat{E}_z^{n+1} + \hat{E}_z^n\right) \quad (24)\end{aligned}$$

It can be observed that $\hat{H}_y^*$ and $\hat{H}_z^{n+1}$ are coupled which cannot be updated explicitly. By substituting $\hat{H}_y^*$ and $\hat{H}_z^{n+1}$ into (21)-(24) for decoupling, one obtains

$$\begin{aligned}&(1 - p_{3hz}p_{3ez}\partial_z\partial_z)\,\hat{E}_x^* \\ &= (c_1 + p_{3hz}p_{3ez}\partial_z\partial_z)\,\hat{E}_x^n \\ &\quad - 2p_{3hx}p_{3ez}\partial_z\partial_x\hat{E}_z^n - (1 + c_1)\,p_{3ez}\partial_z\hat{H}_y^n + 2p_{3ey}\partial_y\hat{H}_z^n \\ &\quad + p_{1ey}\hat{F}_{xy1}^n + p_{2ey}\hat{F}_{xy2}^n - p_{1ez}\hat{F}_{xz1}^n - p_{2ez}\hat{F}_{xz2}^n \\ &\quad - p_{1hx}p_{3ez}\partial_z\hat{G}_{yx1}^n \\ &\quad - p_{2hx}p_{3ez}\partial_z\hat{G}_{yx2}^n + p_{1hz}p_{3ez}\partial_z\hat{G}_{yz1}^n + p_{2hz}p_{3ez}\partial_z\hat{G}_{yz2}^n \quad (25)\\ &\left(1 - p_{3hy}p_{3ey}\partial_y\partial_y\right)\hat{E}_x^{n+1} \\ &= \hat{E}_x^* - p_{3hy}p_{3ex}\partial_x\partial_y\left(\hat{E}_y^n + \hat{E}_y^*\right) \\ &\quad + 2p_{3hy}p_{3ey}\partial_y\partial_y\hat{E}_x^n + p_{1hx}p_{3ey}\partial_y\hat{G}_{zx1}^n + p_{2hx}p_{3ey}\partial_y\hat{G}_{zx2}^n \\ &\quad - p_{1hy}p_{3ey}\partial_y\hat{G}_{zy1}^n - p_{2hy}p_{3ey}\partial_y\hat{G}_{zy2}^n \quad (26)\end{aligned}$$

It can be observed that tri-diagonal matrices are formed at left sides of (25) and (26) which can be updated by employing the Thomas decomposition [21].

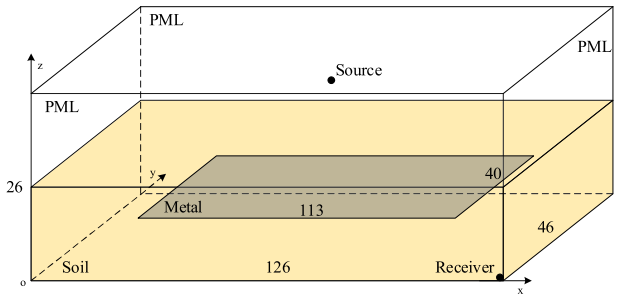

FIGURE 1. The sketch picture of the half-space soil/metal plate problem and its computational domain.

III. NUMERICAL RESULTS AND DISCUSSION

In order to further demonstrate the efficiency and effectiveness of the proposed algorithm, numerical examples including the half-space soil/metal plate problem and the target characteristic of metal sphere model are carried out. To demonstrate the effectiveness of the proposed scheme, the higher order PML based on the conventional FDTD algorithm in [32] (FDTD-PML), CNDS based PML in [19] (CNDS-PML), CNAFS based PML in [20] (CNAFS-PML) are chosen as examples for comparison.

A. HALF-SPACE SOIL/METAL PLATE PROBLEM

The sketch picture and detail parameters of half-space soil/metal plate problem is shown in Fig. 1.

As is shown in Fig. 1 that the whole computational domain has dimensions of $126\Delta x \times 46\Delta y \times 26\Delta z$ in each directions. Half of the vertical direction along z-direction is filled with soil which can be expressed by the lossy media with the parameters of $\varepsilon_r = 7.73$ and $\sigma = 0.273$ S/m. The metal plate has dimensions of $113\Delta x \times 40\Delta y \times 1\Delta z$ which can be expressed by the perfect E conductor (PEC). The metal plate is located at the quarter along vertical direction of z-direction. The source which is located at the three-quarter of vertical z-direction is a modulated Gaussian pulse with the center frequency and bandwidth of 0.75 GHz and 0.25 GHz, respectively. The modulated Gaussian pulse can be expressed by the following forms as

$$J_z(t) = \cos\left[2\pi f_c (t - t_0)\right] \exp\left[-\frac{2\pi (t - t_0)^2}{\tau^2}\right] \quad (27)$$

where f_c is the center frequency and τ determinates the bandwidth. The receiver is located at the left bottom corner with the distance of 1 cell from three sides of the PML regions. The main purpose for the receiver is to observe the waveform and evaluate the absorbing performance. At each boundaries, 10-cell-PML is employed to absorb outgoing waves and reduce the wave reflections. Within the PML regions, the parameters are chosen to obtain the best absorbing performance. The parameters of FDTD-PML and CE-CNDS-HO-PML are chosen as $\kappa_{\eta 1} = 20$, $\alpha_{\eta 1} = 0.6$, $m_{\eta 1} = 2$, $\sigma_{\eta 1\_\max} = 1.6\sigma_{\eta 1\_opt}$, $\kappa_{\eta 2} = 5$, $\alpha_{\eta 2} = 0.7$, $m_{\eta 2} = 3$ and $\sigma_{\eta 2\_\max} = 0.05\sigma_{\eta 2\_opt}$, where

$$\sigma_{\eta n\_opt} = (m_{\eta n} + 1)/(150\pi\Delta\eta) \quad (28)$$

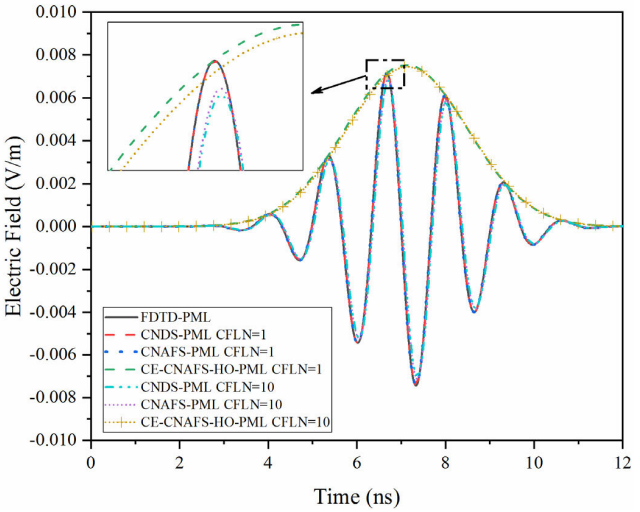

FIGURE 2. The waveform obtained by different PML algorithms with different CFLNs and its partial enlargement.

The parameters of CNDS-PML and CNAFS-PML are $\kappa_\eta = 12$, $\alpha_\eta = 1.4$, $m_\eta = 2$ and $\sigma_{\eta\_\max} = 2.0\sigma_{\eta\_opt}$. The mesh sizes are chosen as $\Delta x = \Delta y = \Delta z = \Delta = 3$ mm. The maximum time step of the conventional FDTD algorithm which satisfies the CFL condition is 5.77 ps. According to CE method, the time step of CE method ($\Delta t_{\max}^{CE}$) is 23.08 ps which is four time larger than $\Delta t_{\max}^{FDTD}$ [5]. The CFL number (CFLN) is defended as $CFLN = \Delta t / \Delta t_{\max}$, where Δt is the time step of the unconditionally stable algorithm. Figure 2 shows the waveform obtained by different PML algorithms with different CFLNs and its partial enlargement.

As shown in Fig. 2, the envelope can be directly obtained by employing the proposed CE method. Furthermore, it can be concluded that the computational accuracy decreases with the increment of CFLNs. The reason is that numerical dispersion increases with the increment of CFLNs resulting in such phenomenon. From the partial enlargement, it can be observed that the proposed scheme shows less shifting compared with the CNDS- and CNAFS-PMLs indicating that the proposed scheme holds higher accuracy especially with larger CFLNs. Such phenomenon indicates the effectiveness of the proposed algorithm.

The effectiveness of PML algorithm can be reflected not only by the accuracy but also by the absorption. The absorbing performance of the PML regions can be expressed by the relative reflection error which can be defined as

$$R_{dB}(t) = 20\log_{10}\left[\left|E_z^t(t) - E_z^r(t)\right| / \left|\max\{E_z^r(t)\}\right|\right] \quad (29)$$

where $E_z^t(t)$ is the waveform directly obtained from the receiver and $E_z^r(t)$ is the reference solution which can be obtained by enlarging the computational domain and terminating by 64-cell-PML. During the simulation of the reference solution, the reflected waves from the boundaries

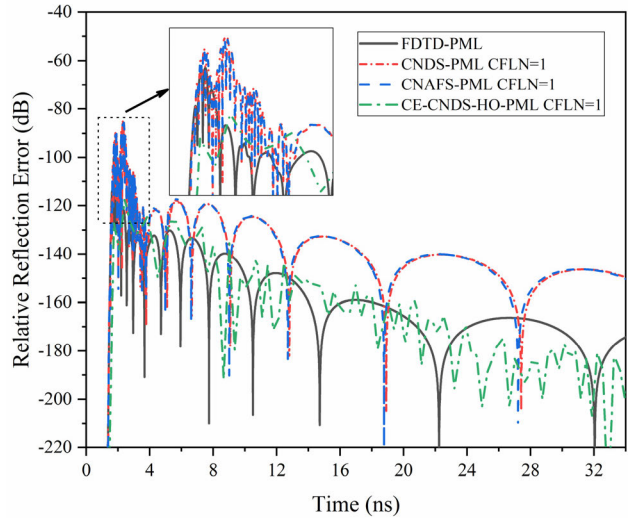

(a)

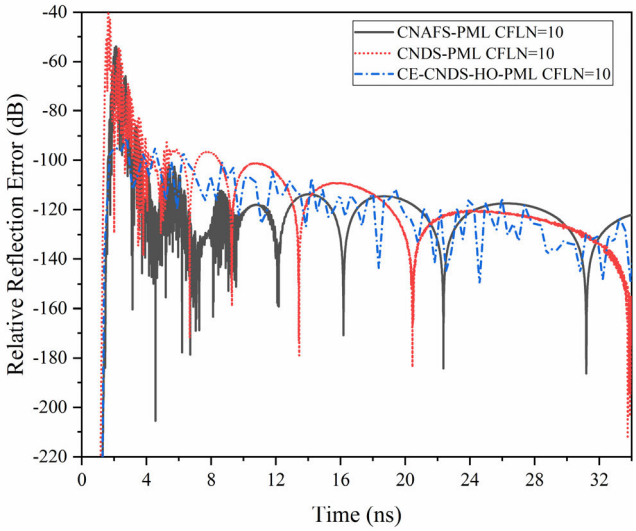

(b)

FIGURE 3. The relative reflection error versus time obtained by different PML algorithms with different CFLNs (a) FDTD-PML, CNDS-PML, CNAFS-PML, and CE-CNDS-HO-PML CFLN=1 (b) CNDS-PML, CNAFS-PML, and CE-CNDS-HO-PML CFLN=10.

cannot reach the receiver. The reason is that the computational domain is large enough and the PML is thick enough resulting in the neglecting of reflected waves. Figure 3 shows the relative reflection error versus time obtained by different PML algorithms with different CFLNs. For clearance, 6000 steps during the simulation time of 34 ns is shown respectively in each figure.

The absorbing performance can be reflected by the maximum value of relative reflection error (MRRE), as shown in Table 1. It can be concluded from Table 1 and Fig. 3 that the CNDS- and CNAFS-PMLs hold the similar absorbing performance when CFLN=1. It can be observed that the MRRE and the late-time reflections can be decreased significantly by employing the higher order schemes. Among the higher order schemes, the proposed CE-CNDS-HO-PML can obtain better absorbing performance and lower late-time reflections

TABLE 1. CPU time, CFLNs, iteration steps, consumption memory, MRRE and time reduction with different PML algorithms.

PML Algorithms	CFLN	Steps	Memory (MB)	CPU Time (s)	Reduction (%)	MRRE (dB)
FDTD-PML	1	32768	67.2	803	-	-108.7
CNDS-PML	1	32768	98.6	2081	-159.2	-84.5
CNAFS-PML	1	32768	103.5	3718	-363.0	-84.5
Proposed	1	8192	152.8	684	14.8	-117.5
CNDS-PML	10	3277	98.6	492	38.7	-40.3
CNAFS-PML	10	3277	103.5	501	37.6	-53.7
Proposed	10	820	152.8	217	72.9	-91.8

compared with FDTD-PML. Thus, it can be concluded that the absorption of proposed scheme is better than FDTD-, CNAFS- and CNDS-PMLs indicating the effectiveness of the proposal.

When CFLN=10, the CNAFS-PML shows better performance compared with CNDS-PML indicating the advantages of CNAFS-PML in terms of the absorption and accuracy. The absorbing performance of both CNDS- and CNAFS-PMLs become worse with larger CFLNs. It can be observed that the MRRE can be significantly reduced by the proposed CE-CNDS-HO-PML scheme. Overall, the absorbing performance can be improved significantly by employing the proposed scheme. The CPU time, CFLNs, iteration steps, consumption memory, MRRE and time reduction with different PML algorithms are shown in Table 1.

It can be concluded from Fig. 3 and Table 1 that absorbing performance can be significantly improved by employing the proposed scheme. Especially, the MRRE of proposed scheme is 9.8 dB lower than FDTD-PML with the time reduction of 14.8 %. Thus, for FDTD-PML, the proposed scheme receives better performance both in absorption and efficiency when CFLN=1. Moreover, the CPU time reduces by 72.9 % when CFLN=10 compared with the FDTD-PML. The proposed scheme can receive both better absorption and improved efficiency compared with the CNDS- and CNAFS-PMLs with larger CFLNs. Furthermore, the proposed scheme with CFLN=10 can save much CPU time with considerable absorption which is better than that of the CNAFS- and CNDS-PMLs when CFLN=1. As can be concluded that the efficiency of unconditionally stable algorithms can be can be improved by employing larger CFLNs. The reason is that larger time steps are employed to decrease the total number of iterations resulting in the improvement efficiency. The time step of the CE method is much larger than the conventional time step of the FDTD method. Thus, the total iteration step of the CE method can be decreased resulting in the improvement of efficiency.

B. TARGET CHARACTERISTIC OF METAL SPHERE MODEL

The accuracy, efficiency and absorption of the proposed CE-CNDS-HO-PML are testified through the target characteristic numerical example which can be reflected by the radar cross section (RCS). The computational domain and its detail parameters are shown in Fig. 4.

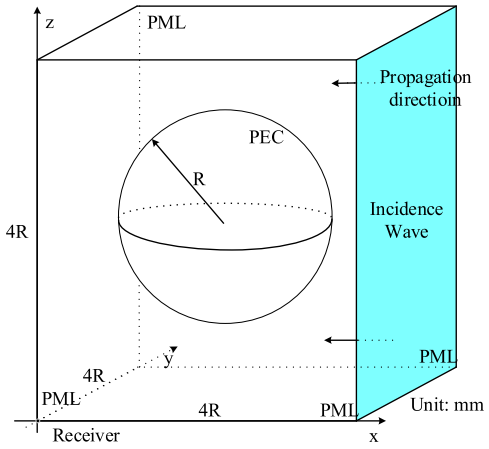

FIGURE 4. The sketch picture and detail parameters of target characteristic numerical example.

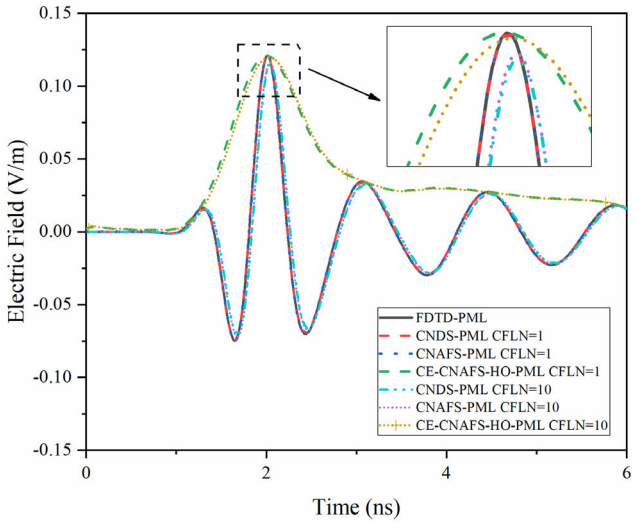

FIGURE 5. The waveform obtained by different PML algorithms with different CFLNs and its partial enlargement.

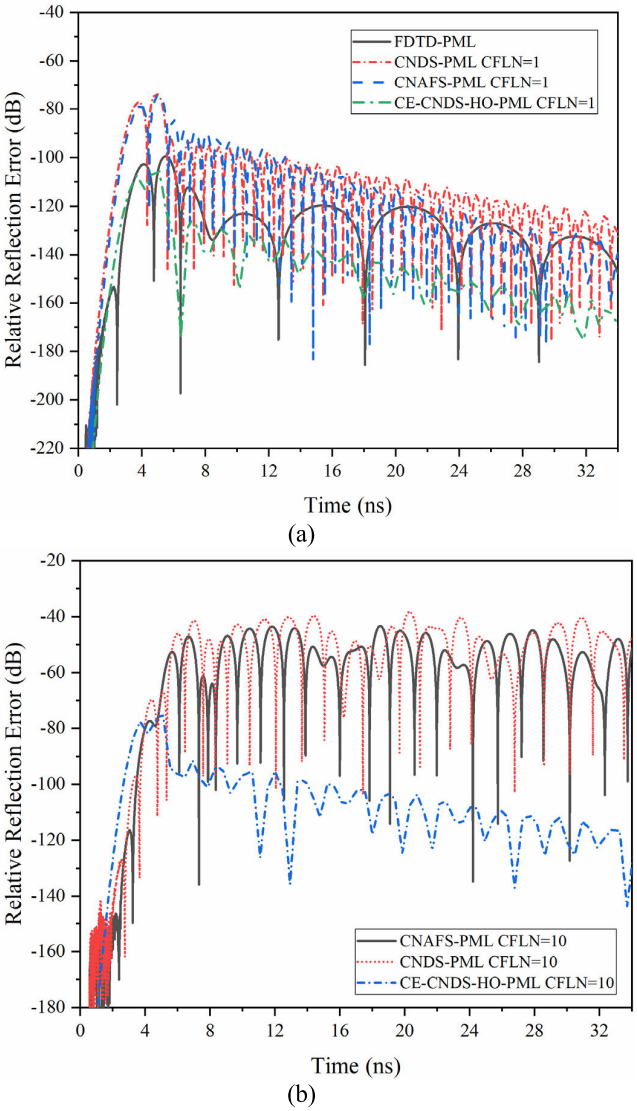

FIGURE 6. The relative reflection error versus time obtained by different PML algorithms with different CFLNs in the metal sphere model (a) FDTD-PML, CNDS-PML, CNAFS-PML, and CE-CNDS-HO-PML CFLN=1 (b) CNDS-PML, CNAFS-PML, and CE-CNDS-HO-PML CFLN=10.

As can be observed that the sphere model is located at the center of the domain. The sphere model has the radius of R=50 mm which can be regarded as PEC material. The whole cubic computational domain has dimension of $4R \times 4R \times 4R$ in each directions. The wave incidents along the negative side along x-direction. The source is a modulated Gaussian pulse with the center frequency of 1.4 GHz and bandwidth of 1 GHz. The receiver is located at the corner of the domain with the distance of 1 cell from three sides of the PML regions.

It has been testified that such condition can obtain the worst absorbing performance [33]. All sides of the boundaries are terminated with 10-cell-PML to absorb outgoing waves and reduce the wave reflection. The parameters inside the PML regions are chosen to obtain the best absorbing performance both in the time domain and in the frequency domain. The parameters of FDTD-PML and CE-CNDS-HO-PML are chosen as $\kappa_{\eta 1} = 12$, $\alpha_{\eta 1} = 1.1$, $\sigma_{\eta 1\_\max} = 0.4\sigma_{\eta 1\_opt}$, $\kappa_{\eta 2} = 2$, $\alpha_{\eta 2} = 0.2$, $m_{\eta 2} = 2$ and $\sigma_{\eta 2\_\max} = 1.0\sigma_{\eta 2\_opt}$. The parameters of CNDS-PML and CNAFS-PML are $\kappa_\eta = 8$, $\alpha_\eta = 0.9$, $m_\eta = 4$ and $\sigma_{\eta\_\max} = 1.6\sigma_{\eta\_opt}$.

The mesh sizes can be chosen as $\Delta x = \Delta y = \Delta z = \Delta = 1.25$ mm. The time step of the conventional FDTD algorithm is $\Delta t_{\max}^{FDTD} = 2.4$ ps. The time step of the CE method is $\Delta t_{\max}^{CE} = 5.76$ ps, which is 2.4 times larger than $\Delta t_{\max}^{FDTD}$ [5]. Figure 5 shows the waveform obtained by different PML algorithms with different CFLNs and its partial enlargement. As can be observed that the waveform obtained by different algorithms when CFLN=1 are overlapped indicating they hold the similar accuracy. By employing the CE algorithm, it can be observed that the envelope can be obtained which is overlapped with the edge of waveform. As can be observed that the accuracy decreases with the increment of CFLNs due to the increment of numerical dispersive error. As shown in the partial enlargement, the CE algorithm shows less shifting

TABLE 2. CPU time, CFLNs, iteration steps, consumption memory, MRRE and time reduction with different PML algorithms.

PML Algorithms	CFLN	Steps	Memory (MB)	CPU Time (M)	Reduction (%)	MRRE (dB)
FDTD-PML	1	32768	947.1	47.9	-	-99.4
CNDS-PML	1	32768	1366.2	94.0	-96.2	-73.7
CNAFS-PML	1	32768	1407.5	101.6	-112.1	-74.1
Proposed	1	8192	2135.0	40.8	14.8	-106.2
CNDS-PML	10	3277	1366.2	29.1	39.2	-40.3
CNAFS-PML	10	3277	1407.5	32.3	32.6	-44.3
Proposed	10	820	2135.0	11.2	76.6	-68.6

compared with CNDS- and CNAFS-PMLs indicating the proposed scheme shows advantage in terms of accuracy. The absorption can be reflected by the relative reflection error versus time in the time domain. Figure 6 shows relative reflection error versus time obtained by different PML algorithms with different CFLNs in the sphere model.

Through Fig. 6, it can be observed that the relative reflection error is decreased by employing the CNDS- and CNAFS-PMLs with MRRE of -73.7 dB and -74.1 dB, respectively, compared with the FDTD-PML with MRRE of -99.4 dB. By employing the CE method, the MRRE can be improved with the value of -106.2 dB indicating the effectiveness of proposed scheme. The absorption becomes worse with the increment of CFLNs. However, it can be observed that the MRRE can be decreased by 28.3 dB and 24.3 dB by employing the proposed scheme compared with CNDS- and CNAFS-PMLs. In conclusion, the proposed CE-CNDS-HO-PML can obtain better absorption compared with the CNAFS- and CNDS-PMLs. The effectiveness of the proposed scheme can also be reflected by the computational efficiency. Table 2 shows the CPU time, CFLNs, iteration steps, consumption memory, MRRE and time reduction with different PML algorithms.

It can be observed that the CPU time and consumption memory are increased by employing the unconditionally stable CNDS- and CNAFS-PMLs algorithms. The reason is that tri-diagonal matrices must be calculated at each time step resulting in such condition. Although the consumption memory of proposed scheme becomes the highest among these implementations, the CPU time can be significantly decreased by 14.8 % compared with FDTD-PML when CFLN=1. The reason is that the time step in the CE algorithm is terminated by the bandwidth rather than the maximum frequency. Thus, the total iteration steps can be decreased by employing the CE method. When CFLN=10, the proposed scheme can maintain considerable absorption with the time reduction of 76.6 %. Compared with the CNDS- and CNAFS-PMLs, it can be concluded that not only the absorption but also the efficiency can be improved at the same time. This illustrates the effectiveness of the proposed scheme from the aspect of efficiency.

The accuracy of the proposed algorithm and target characteristics can be reflected by the RCS parameters. The main reason for selecting the sphere model during the demonstration is that the RCS of the sphere model has the theoretical solution [35]. Figure 7 shows the RCS versus frequency of the sphere model obtained by different PML algorithms with different CFLNs. It can be observed from Fig. 7 (a) that all implementations are almost overlapped indicating they almost hold the same performance in the frequency domain. From Fig. 7 (b), it can be observed that the computational accuracy decreases with the increment of CFLNs. Compared with the CNDS-PML, the CNAFS-PML shows less shifting indicating that the CNAFS-PML hold the better accuracy compared with the CNDS-PML. Furthermore, the proposed scheme shows the least shifting compared with the theoretical solution indicating it has the best accuracy among these implementations within larger CFLNs.

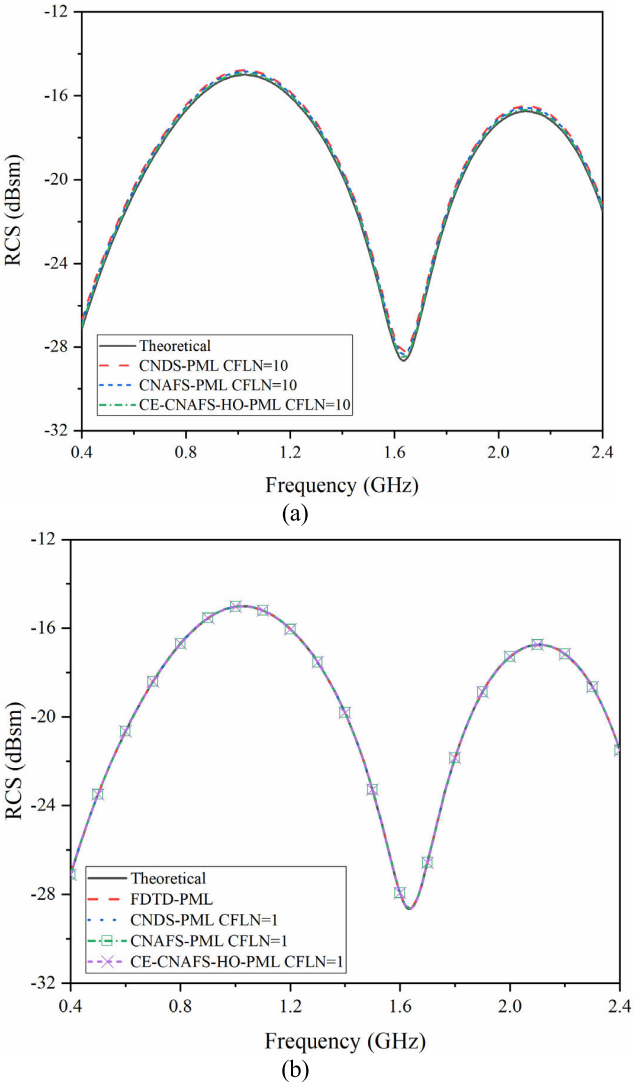

FIGURE 7. The RCS versus frequency obtained by different PML algorithms with different CFLNs in the metal sphere model (a) Theoretical solution, FDTD-PML, CNDS-PML, CNAFS-PML, and CE-CNDS-HO-PML CFLN=1 (b) Theoretical solution, CNDS-PML, CNAFS-PML, and CE-CNDS-HO-PML CFLN=10.

In conclusion, compared with the FDTD-, CNDS- and CNAFS-PML, the proposed scheme can obtain better absorption and efficiency which can be reflected by the MRRE,

CPU time and time reduction. Nowadays, the memory is cheaper than ever before, one cared more on the efficiency and accuracy. Although the proposed scheme occupies a little bit more memory, the efficiency and the accuracy can be improved.

IV. CONCLUSION

Based upon higher order PML formulation, CE method and CNDS algorithm, unconditionally stale CE-CNDS-HO-PML is proposed for bandpass open region problems. The proposed scheme take advantages of CE method, higher order formulation and CNDS algorithm in terms of enhanced absorption, improved efficiency and bandpass simulation in open region problems. Through the resultants, it can be concluded that the proposed scheme is stable and efficient when the time step surpasses far beyond the CFL condition. Most importantly, it can significantly improve the computational efficiency compared with previous work during the bandpass simulation. In the future work, such implementation can be employed into curved boundaries, such as, the spherical coordinate system and column coordinates system, respectively.

REFERENCES

[1] K. Yee, "Numerical solution of initial boundary value problems involving Maxwell's equations in isotropic media," *IEEE Trans. Antennas Propag.*, vol. 14, no. 3, pp. 302–307, May 1966.
[2] Q. Cao and X. Chen, "Analysis of characteristics of two-dimensional Runge-Kutta multiresolution time-domain scheme," *Prog. Electromagn. Res. M*, vol. 13, pp. 217–227, 2010.
[3] W. E. I. Sha, X.-L. Wu, Z.-X. Huang, and M.-S. Chen, "Waveguide simulation using the high order symplectic finite-difference time-domain scheme," *Prog. Electromagn. Res. B*, vol. 13, pp. 237–256, 2009.
[4] Y. Liu, Y.-W. Chen, P. Zhang, and X. Xu, "Implementation and application of the spherical MRTD algorithm," *Prog. Electromagn. Res.*, vol. 139, pp. 577–597, 2013.
[5] J. D. Pursel and P. M. Goggans, "A finite-difference time-domain method for solving electromagnetic problems with bandpass-limited sources," *IEEE Trans. Antennas Propag.*, vol. 47, no. 1, pp. 9–15, Jan. 1999.
[6] C. Ma and Z. Chen, "Dispersion analysis of the three-dimensional complex envelope ADI-FDTD method," *IEEE Trans. Antennas Propag.*, vol. 53, no. 3, pp. 971–976, Mar. 2005.
[7] O. Ramadan, "Unsplit field implicit PML algorithm for complex envelope dispersive LOD-FDTD simulations," *Electron. Lett.*, vol. 43, no. 5, pp. 17–18, Mar. 2007.
[8] K.-Y. Jung, F. L. Teixeira, S. G. Garcia, and R. Lee, "On numerical artifacts of the complex envelope ADI-FDTD method," *IEEE Trans. Antennas Propag.*, vol. 57, no. 2, pp. 491–498, Feb. 2009.
[9] A. Taflove and S. C. Hagness, *Computational Electrodynamics: The Finite-Difference Time-Domain Method*, 3rd ed. Boston, MA, USA: Artech House, 2005.
[10] Y. Yang, R. S. Chen, D. X. Wang, and E. K. N. Yung, "Unconditionally stable Crank-Nicolson finite-different time-domain method for simulation of three-dimensional microwave circuits," *IET Microw., Antennas Propag.*, vol. 1, no. 4, pp. 937–942, Aug. 2007.
[11] J. Li, Y. Yu, and X. Zhao, "Z-transform for unconditional stable Crank-Nicolson FDTD implementation of SC-PML for dispersive debye media," *Electron. Lett.*, vol. 50, no. 25, pp. 1959–1961, Dec. 2014.
[12] J. Li and P. Wu, "Unconditionally stable CNAD- and BT-based CFS-PML implementation for truncating anisotropic magnetic plasma," *IEEE Antennas Wireless Propag. Lett.*, vol. 17, no. 7, pp. 1176–1180, Jul. 2018.
[13] G. Sun and C. W. Trueman, "Approximate Crank-Nicolson scheme for the 2-D finite-difference time-domain method for TEz waves," *IEEE Trans. Ante. Propag.*, vol. 52, no. 11, pp. 2963–2972, Nov. 2004.
[14] G. Sun and C. W. Trueman, "Unconditionally stable Crank-Nicolson scheme for solving two-dimensional Maxwell's equations," *Electron. Lett.*, vol. 39, pp. 595–597, Apr. 2003.
[15] X. Shi and X. Jiang, "Implementation of the Crank-Nicolson Douglas-Gunn finite-difference time domain with complex frequency-shifted perfectly matched layer for modeling unbounded isotropic dispersive media in two dimensions," *Microw. Opt. Technol. Lett.*, vol. 62, no. 3, pp. 1103–1111, Mar. 2020.
[16] G. Sun and C. W. Trueman, "Unconditionally-stable FDTD method based on Crank-Nicolson scheme for solving three-dimensional Maxwell equations," *Electron. Lett.*, vol. 40, no. 10, pp. 589–590, May 2004.
[17] G. Sun and C. W. Trueman, "Efficient implementations of the Crank-Nicolson scheme for the finite-difference time-domain method," *IEEE Trans. Microw. Theory Techn.*, vol. 54, no. 5, pp. 2275–2284, May 2006.
[18] E. L. Tan, "Efficient algorithms for crank–nicolson-based finite-difference time-domain methods," *IEEE Trans. Microw. Theory Techn.*, vol. 56, no. 2, pp. 408–413, Feb. 2008.
[19] H. L. Jiang, L. T. Wu, X. G. Zhang, Q. Wang, P. Y. Wu, C. Liu, and T. J. Cui, "Computationally efficient CN-PML for EM simulations," *IEEE Trans. Microw. Theory Techn.*, vol. 67, no. 12, pp. 4646–4655, Dec. 2019.
[20] H. L. Jiang and T. J. Cui, "Efficient PML implementation for approximate CN-FDTD method," *IEEE Antennas Wireless Propag. Lett.*, vol. 18, no. 4, pp. 698–701, Apr. 2019.
[21] T. Sauer, *Numerical Analysis*, 2rd ed. Boston, MA, USA: Pearson, 2006.
[22] J.-P. Berenger, "A perfectly matched layer for the absorption of electromagnetic waves," *J. Comput. Phys.*, vol. 114, no. 2, pp. 185–200, Oct. 1994.
[23] W. C. Chew and W. H. Weedon, "A 3D perfectly matched medium from modified Maxwell's equations with stretched coordinates," *Microw. Opt. Technol. Lett.*, vol. 7, no. 13, pp. 599–604, Sep. 1994.
[24] M. Kuzuoglu and R. Mittra, "Frequency dependence of the constitutive parameters of causal perfectly matched anisotropic absorbers," *IEEE Microw. Guided Wave Lett.*, vol. 6, no. 12, pp. 447–449, Dec. 1996.
[25] Z. S. Sacks, D. M. Kingsland, R. Lee, and J.-F. Lee, "A perfectly matched anisotropic absorber for use as an absorbing boundary condition," *IEEE Trans. Antennas Propag.*, vol. 43, no. 12, pp. 1460–1463, Dec. 1995.
[26] Y. Liu, P. Zhang, and Y.-W. Chen, "Implementation of the parallel higher-order FDTD with convolution PML," *Prog. Electromagn. Res. Lett.*, vol. 70, pp. 129–138, 2017.
[27] C. L. Wagner and J. L. Young, "FDTD numerical tests of the Convolutional PML at extremely low frequencies," *IEEE Antennas Wireless Propag. Lett.*, vol. 8, pp. 1398–1401, 2009.
[28] D. Correia and J.-M. Jin, "On the development of a higher-order PML," *IEEE Trans. Antennas Propag.*, vol. 53, no. 12, pp. 4157–4163, Dec. 2005.
[29] O. Ramadan, "Complex envelope Crank Nicolson PML algorithm for band-limited electromagnetic applications," *Electron. Lett.*, vol. 42, no. 12, pp. 1325–1326, Nov. 2006.
[30] J. Li and P. Wu, "Unconditionally stable higher order CNAD-PML for left-handed materials," *IEEE Trans. Antennas Propag.*, vol. 67, no. 11, pp. 7156–7161, Nov. 2019.
[31] P. Wu, Y. Xie, and H. Jiang, "Higher order perfectly matched layer for the implicit CNDG-FDTD algorithm," *Int. J. Numer. Model., Electron. Netw., Devices Fields*, vol. 33, no. 5, Sep. 2020, Art. no. e2750.
[32] J. Li, Q. Yang, P. Niu, and N. Feng, "An efficient implementation of the higher-order PML based on the Z-transform method," in *Proc. IEEE Int. Conf. Microw. Technol. Comput. Electromagn.*, May 2011, pp. 414–417.
[33] J. Li, L.-X. Guo, and H. Zeng, "FDTD investigation on bistatic scattering from a target above two-layered rough surfaces using UPML absorbing condition," *Prog. Electromagn. Res.*, vol. 88, pp. 197–211, 2008.
[34] A. M. Shreim and M. F. Hadi, "Integral PML absorbing boundary conditions for the high-order M24 FDTD algorithm," *Prog. Electromagn. Res.*, vol. 76, pp. 141–152, 2007.
[35] K. Umashankar, A. Taflove, and S. Rao, "Electromagnetic scattering by arbitrary shaped three-dimensional homogeneous lossy dielectric objects," *IEEE Trans. Antennas Propag.*, vol. 34, no. 6, pp. 758–766, Jun. 1986.

SHIHONG WU was born in Yingkou, Liaoning, China, in 1966. He received the B.S. degree from the School of Construction Machinery, Shandong Jiaotong University, Jinan, China, and the M.S. degree from the Kyoto University of Technology and Fiber, Kyoto, Japan, and the Ph.D. degree in advanced materials science from the Department of Process Science, Kyoto University of Technology and Fiber, in March 2007.

From June 2001 to March 2002 and April 2002 to March 2004, he was a Graduate Student of advanced materials science with the Department of Process Science, Kyoto University of Technology and Fiber. His research interests include computational electromagnetics and electrical and mechanical properties of CNF/UPR nanocomposites.

YUNYUN DONG was born in August 1980. She received the bachelor's degree in automation and the master's degree in control theory and control engineering from Jinan University, in July 2004 and July 2008, respectively. From August 2004 to July 2005, she was a Teacher with the Linqing Technical School, Shandong. Since July 2008, she has been a Teacher with Yantai Nanshan University, and an Associate Professor of control theory and control engineering.

FENG SU was born in 1981. She received the master's degree in microelectronics and solid state electronics from Southwest Jiaotong University, in 2008. She is currently an Associate Professor with the Department of Electrical and Electronic Engineering, Institute of Technology, giving lectures on circuit principle, digital electronic technology, automatic detection technology, and so on.

LINING LIU was born in April 1980. She received the bachelor's degree in thermal energy and power engineering, the master's degree in thermal engineering and the Ph.D. degree in power engineering and engineering thermophysics from Shandong University, in July 2003, July 2006, and March 2019, respectively.

Since July 2006, she has been a Teacher with Yantai Nanshan University. She is currently an Associate Professor. She is mainly engaged in teaching and scientific research of energy and power engineering. Her research interests include energy saving of thermal equipment and automobile aerodynamics.

XIANGGUANG CHEN was born in September 1953. He graduated from the Department of Chemical Engineering, Beijing Institute of Technology, in 1978. He received the master's degree in engineering from the Department of Chemical Engineering, Beijing Institute of Technology, in April 1986, and the Ph.D. degree in engineering from the School of Chemical Engineering and Materials, Beijing University of Technology, in July 2000.

He was with the School of Chemical Engineering and Materials, Beijing University of Technology, a Lecturer from April 1986 to June 1995, an Associate Professor from July 1995 to June 2000, a Professor, and has been a Doctoral Supervisor, since November 2002. Since June 2002, he has been the Director of the Department of Chemical Engineering and Control, School of Chemical Engineering and Environment, Beijing University of technology, where he has been a Professor of process equipment and control engineering, School of Chemical Engineering and Environment, since June 2006. As a Senior Visiting Scholar, he studied at the Brandenburg University of Technology Cottbus, Germany, from 1995 to 1996, and the University of Leicester, U.K., from 2004 to 2005. He is currently a Professor with the Beijing University of Technology and a Doctoral Supervisor of detection technology and automation device. His research interests include: control science and engineering, chemical engineering and technology.

Dr. Chen is also a member of the Communist Party of China.